International Journal of Nanomedicine

Dovepress

open access to scientific and medical research

Open Access Full Text Article

ORIGINAL RESEARCH

Bone Marrow Mesenchymal Stem Cell-Derived Nanovesicles Containing H8 Improve Hepatic Glucose and Lipid Metabolism and Exert Ameliorative Effects in Type 2 Diabetes

Meng Zhang[1,2], Qi Yuan[1], Peiwen Wang[1], Fan Zhang[1], Dan Wu[1], He Bai[1], Jieting Liu[1], Haifeng Liu[1], Xiaohuan Yuan[1]

[1]College of Life Science, Mudanjiang Medical University, Mudanjiang, People's Republic of China; [2]The First Hospital of Qiqihar, Qiqihar, People's Republic of China

Correspondence: Xiaohuan Yuan, College of Life Science, Mudanjiang Medical University, No. 3 Tongxiang Road, Mudanjiang, 157011, People's Republic of China, Tel/Fax +86-453-6984401, Email yuanxiaohuan@mdjmu.edu.cn

Purpose: Nanovesicles (NVs) derived from bone mesenchymal stem cells (BMSCs) as drug delivery systems are considered an effective therapeutic strategy for diabetes. However, its mechanism of action remains unclear. Here, we evaluated the efficacy and molecular mechanism of BMSC-derived NVs carrying the curcumin analog H8 (H8-BMSCs-NVs) on hepatic glucose and lipid metabolism in type 2 diabetes (T2D).

Subjects and Methods: Mouse BMSCs were isolated by collagenase digestion and H8-BMSCs-NVs were prepared by microvesicle extrusion. The effects of H8-BMSCs-NVs on hepatic glucose and lipid metabolism were observed in a T2D mouse model and a HepG2 cell insulin resistance model. To evaluate changes in potential signaling pathways, the PI3K/AKT/AMPK signaling pathway and expression levels of G6P and PEPCK were assessed by Western blotting.

Results: H8-BMSCs-NVs effectively improved lipid accumulation in liver tissues and restored liver dysfunction in T2D mice. Meanwhile, H8-BMSCs-NVs effectively inhibited intracellular lipid accumulation in the insulin resistance models of HepG2 cells. Mechanistic studies showed that H8-BMSCs-NVs activated the PI3K/AKT/AMPK signaling pathway and decreased the expression levels of G6P and PEPCK.

Conclusion: These findings demonstrate that H8-BMSCs-NVs improved hepatic glucose and lipid metabolism in T2D mice by activating the PI3K/AKT/AMPK signaling pathway, which provides novel evidence suggesting the potential of H8-BMSCs-NVs in the clinically treatment of T2D patients.

Keywords: bone mesenchymal stem cell, nanovesicles, curcumin analogue H8, type 2 diabetes

Introduction

Dramatic changes in lifestyle and environment have enabled diabetes to rapidly become a global epidemic in the 21st century, with attendant complications posing a major threat to global health.[1–3] The global prevalence of diabetes is expected to increase to 700 million by 2045, compared to an estimated 463 million in 2019.[4] Type 2 diabetes (T2D), which accounts for 90% of diabetes cases worldwide, is a global epidemic metabolic disease characterized by hyperglycemia and insulin resistance in target tissues.[5,6] Controlling hyperglycemia and improving insulin resistance are two key steps in T2D treatment. Although conventional insulin sensitizers, including rosiglitazone, metformin, and the antioxidant α-lipoic acid, have been shown to improve insulin sensitivity in target tissues, no single drug has been found to treat T2D completely.[7] Therefore, more effective strategies to reduce blood glucose levels and promote insulin sensitivity through novel mechanisms are urgently required.

Received: 23 January 2024
Accepted: 20 June 2024
Published: 3 July 2024

Curcumin is a yellow polyphenol compound derived from turmeric plants and is commonly used as a spice, dye, and medicinal plant. Previous studies have revealed that curcumin has numerous pharmacological properties, including anti-inflammatory, anti-bacterial, anti-cancer, and anti-diabetic activities.[8–10] Hajavi et al demonstrated that curcumin could improve insulin resistance and reduce glucose levels in T2D patients.[11] In addition, supplementation of curcumin improved lipid profile and increased total antioxidant capacity of patients with T2D.[12,13] However, the therapeutic applications of curcumin are limited by its extremely low solubility in aqueous buffers, instability in bodily fluids, and rapid metabolism. To overcome these defects, we removed the unstable diketone structure of its parent compound and introduced a more stable cyclopentanone structure to construct the curcumin analog (2E,5E)-2,5-bis[2-fluoro-6-(trifluoromethyl)benzylidene] cyclopentanone (compound number: H8).[14] H8 further increased the stability and pharmacokinetic properties of curcumin by maintaining and enhancing its original function.[15] However, its role and molecular mechanisms in T2D require further investigation.

Bone mesenchymal stem cells (BMSCs) are multipotent stem cells with the ability to self-renew, which makes them attractive for the treatment of many diseases.[16] Recently, BMSCs have been considered to exhibit potential immunomodulatory and anti-inflammatory properties through their paracrine effects,[17,18] which are mainly mediated by extracellular vesicles derived by BMSCs. Nanovesicles (NVs) are extracellular vesicles that typically range in diameter from 30 nm to 150 nm. NVs have several advantages over cells, including effectiveness through systemic delivery, and capability of crossing the blood-brain barrier, making them promising vectors for drug delivery.[19,20] Previous studies have confirmed that NVs improve diabetes by regulating the glucose metabolism and insulin secretion.[21] Additionally, NVs have been investigated as potential drug delivery systems for diabetes. Several studies have demonstrated the successful delivery of antidiabetic drugs using NVs to modulate glucose metabolism and insulin sensitivity.[22,23] However, the therapeutic effects of H8 in complex with NVs in T2D have not been investigated and require further investigation.

In this study, we generated bone marrow stem cell nanovesicles containing H8 (H8-BMSCs-NVs). We established a mouse T2D model using a high-fat diet (HFD) combined with streptozotocin (STZ) and established palmitic acid (PA)- and oleic acid (OA)-induced insulin resistance in HepG2 cells. We evaluated the effects of H8-BMSCs-NVs on hepatic glucose and lipid metabolism in vitro and in vivo. Finally, we demonstrated that H8-BMSCs-NVs decreased the expression levels of G6P and PEPCK by activating the PI3K/AKT/AMPK signaling pathway. In summary, our results provide new ideas and a scientific basis for H8-BMSCs-NVs intervention strategies for T2D.

Materials and Methods

Extraction and Identification of BMSCs

According to the previously reported method of BMSCs extraction,[24] C57BL/6J neonatal mice within 0–3 days were taken, and the femur and tibia of the extremities of the neonatal mice were transferred to type I collagenase solution (100 mg type I collagenase was dissolved in a mixture of 32 mL PBS and 8 mL FBS) for digestion and cell isolation. The cells were cultured in a cell incubator (5% CO_2, 37 °C) for 1–2 days, and their morphology and growth of cells were observed under a microscope. When the cell fusion degree was approximately 80%-90%, the cells were passaged, and third-generation cells were used for follow-up experiments. BMSCs were evaluated for pluripotency, lipogenesis, osteogenesis, and chondrogenesis of BMSCs were evaluated.

Preparation of NVs

After the stem cells were isolated for identification, stem cells of more than three generations were cultured with 15 μM H8 solution (dissolved in Dimethyl sulfoxide) for 24 hours. The mesenchymal stem cells of the third generation and above were digested in a 15 mL centrifuge tube, centrifuged at 11,000 r/min for 5 min, the supernatant was discarded, and the cells were re-suspended using PBS (pH=7.4). BMSCs and H8-BMSCs cell suspensions were successively extruded through 5 μm, 1 μm and 0.2 μm polycarbonate membranes using a microvesicle extruder, and each polycarbonate membrane was extruded 15 times. The extruded sample was centrifuged (10,000 g, 10 min) to remove the cell debris and microcapsules. The centrifuged sample was concentrated at 1000 g in a centrifugal filter (100 kDa) for 15 min, then resuspended in the same amount of PBS, infrared was used to verify the presence of H8 in this NVs, and finally stored at −80°C.

Cell Culture

The HepG2 cell line was purchased from Procell Life Sciences Technology Co., LTD. (Hepatocellular Cancer cell line, CL-0103). It was cultured in DMEM medium (Gibco) containing 10% fetal bovine serum (FBS) and 1% penicillin/streptomycin solution(Biosharp). The culture conditions were 37°C, 5% CO2. The cells were passed with trypsin-EDTA. After the cells were inoculated in a 6-well plate with 70% fusion, the cells were placed overnight in serum-free DMEM containing normal glucose. Cells incubated with 5.5 mM D-glucose were used as control group. T2DM was simulated by 30 mM glucose plus 100 nM insulin (HGHI) for 24 h.

Cell Viability

Cell proliferation was detected using a methyl thiazolyl tetrazolium (MTT) assay. BMSCs Cells with exponential growth were inoculated into 96-well plates, different concentrations of H8 solution were used for 24h or 48h, or use different concentrations of BMSCs-NVs and H8-BMSCs-NVs for 24h, 10 μL of MTT solution was added to each well after drug incubation. After incubation for 4 h, 150 μL of dimethyl sulfoxide (DMSO) was added to dissolve the formaldehyde crystals, and the light absorption value was measured at 490 nm.

Live/Dead Cell Staining

HepG2 cells treated with different concentrations of H8 were seeded in 24-well plates, each well was added with 250 μL of Calcein AM/PI detection solution, and incubated at 37°C for 30 min under a fluorescence microscope. (Calcein AM is green fluorescence, Ex/Em=494/517 nm; PI is red fluorescence, Ex/Em=535/617nm). Avoid light during the whole process.

The Construction of T2D Model

Thirty 4-week-old male C57BL/6J mice were randomly divided into five groups: blank group (con), type 2 diabetes group (Dia), H8 treatment group (H8), BMSCs-NVs treatment group (BMSCs-NVs), and H8-BMSCs-NVS treatment group (H8-BMSCS-NVS), with six mice per group. C57BL/6J mice in the control group were fed a maintenance diet, while the, H8 group, and H8-BMSCS-NVS groups were fed a high-fat diet (HFD) for 12 weeks. A 50 mg/kg streptozotocin (STZ) solution fully dissolved in sodium citrate buffer was intraperitoneally injected the next day, and the mice in the control group were intraperitoneally injected with equal doses of sodium citrate buffer. The fasting blood glucose of mice was measured after 3 days, and fasting blood glucose ≥11.1 mmol/L for 3 consecutive days, indicating that the T2D model was successfully established. The H8, BMSC-NV, and H8-BMSCS-NVS groups were treated for eight weeks. H8 group was intraperitoneally injected with 1% dissolved H8 (0.35 mg/kg) every 4 days, BMSCs-NVs group and H8-BMSCS-NVS group were intraperitoneally injected with NVs (100 μg/mL) every 4 days for 8 weeks. The H8-BMSCs-NVS treatment group were treated with PI3K inhibitor[25] (LY294002, 1.2 mg/kg/day) for 4 weeks. All animal experiments followed the ethical guidelines stated in the "Guidelines for the Care and Use of Laboratory Animals" approved by the Ethics Committee of Mudanjiang Medical College ((2011) 04-2018070603-3015).

Intraperitoneal Glucose Tolerance Test and Insulin Tolerance Test

The Intraperitoneal glucose tolerance test (IPGTT) and intraperitoneal insulin tolerance test (IPITT) were administered to overnight-fasted mice via intraperitoneal injections of 2 g/kg glucose or 1U/kg insulin, respectively. To test glucose tolerance,[26] the mice were restricted to food for 12 hours before receiving an intraperitoneal administration with a glucose load of 2 g/kg. Their blood sugar was measured from the tail tip using a glucose meter (Accu-chek®, Roche) before (0 min) and 15, 30, 60, and 120 min after glucose-loaded administration. After 2 days of recovery, the mice were fasted for 4 hours to test insulin resistance, and the mice received 1U/kg insulin (Humulin R, Eli Lilly) intraperitoneally, and blood glucose was measured before (0 min) and 5, 10, 15, 20, 25, 30, and 60 min after insulin administration. Based on the AUC, we evaluated the effective use of insulin in mice to determine the extent of insulin resistance.

Histological Analysis

Liver tissue was dissected and fixed with 4% PFA. Paraffin-embedded liver sections were then cut into 4μm slices after dewaxing and dewatering, stained with hematoxylin and eosin (H&E), Masson's trichromee (Beyotime), and Sirius Red (Beyotime). Frozen sections were prepared and stained with the Oil Red O (Beyotime) working solution.

Enzyme Linked Immunosorbent Assay (ELISA) of Cytokines

For serum examination, the mice were anesthetized and whole peripheral blood was obtained from the retro-orbital venous plexus. Serum was obtained by centrifugation at 3000 rpm for 10 min. For tissue lysis examination, liver tissue was homogenized in a frozen lysis buffer containing protease inhibitors and centrifuged at 2000 rpm for 5 min. The concentrations of interleukin-6 (IL-6), IL-1β, TNF-α, IL-10, and IL-11 in the serum and liver lysates were measured using mouse ELISA kits according to the manufacturer's instructions (Cloud-Clone Corp., Wuhan, China).

NVs Uptake in vitro

HepG2 cells were inoculated in confocal laser culture dishes with a density of 1×10^6 cells per dish. After HepG2 cells were attached to the wall, BMSCs-NVs and H8-BMSCs-NVs solutions containing 10 μg/mL were put into 1.5mL EP tube, and PKH26 (2×10^{-6}m, Shanghai Maokang Biotechnology, MX4021) dye solution was added into the EP tube. After incubation at 37°C for 10 min, BMSCs-NVs and H8-BMSCs-NVs containing PKH26 dye solution[27] were added to the confocal laser culture dish inoculated HepG2 cells for co-incubation. After 12 h, the confocal laser petri dish was taken out and washed 3 times with PBS (pre-heated at 37°C), and appropriate 4% paraformaldehyde solution was fixed for 10 min, then washed twice with PBS (30 s/ times), Triton100 (0.5%) for 2 min, and washed twice with PBS (30 s/ times). Phalloidin (Shanghai Maokang Biotechnology, MX4402) staining (in dark) was incubated at 37°C for 30min, washed with PBS twice (30 s/ time), DAPI staining for 2 min, and cleaned with PBS for 3 times. After that, the uptake of BMSCs-NVs and H8-BMSCs-NVs by HepG2 cells was observed under confocal laser microscope and images were collected.

Biochemical Assays

Alanine aminotransferase (ALT), aspartate aminotransferase (AST), high-density lipoprotein cholesterol (HDL-C), low-density lipoprotein cholesterol (LDL-C), triglyceride (TG), and total cholesterol (TC) levels were measured using kits from the Nanjing Jiancheng Bioengineering Institute (Nanjing, China). According to the kit instructions, mouse serum samples, liver tissue samples after centrifugation supernatant and HepG2 cell broken homogenate were mixed with the working liquid in each kit, incubated at 37°C for corresponding time, and TC and TG were measured at 500 nm for light absorption values. The light absorption values of HDL-C and LDL-C were measured at 600 nm, AST and ALT were measured at 510 nm.

Western Blot Analysis

The HepG2 cells, BMSCs and liver tissue were lysed using RIPA buffer (Solarbio) supplemented with a mixture of protease and phosphatase inhibitors ABC, full grinding, and then centrifuged for 120,000r for 15 min at 4 °C, take the supernatant. The protein concentration of the cells or tissue samples was determined using a bicinchoninic acid (BCA) protein assay kit (Beyotime, Beijing, China). Total protein was electrophoresed using 10% sodium dodecyl sulfate-polyacrylamide gel electrophoresis and transferred onto PVDF membranes. After blocking with skimmed milk (5%), followed by cultivation with the primary antibodies at 4 degrees overnight. The primary antibodies used were anti-calnexin (AF5362, 1:1000, Affinity), anti-CD9 (AF5139, 1:1000, Affinity), anti-CD63 (AF5117, 1:1000, Affinity), anti-PI3K (AF6241, 1:1000, Affinity), anti-p-PI3K (AF3241, 1:1000, Affinity), anti-AKT (AF6259, 1:1000, Affinity), anti-p-AKT (AF0016, 1:1000, Affinity), anti-AMPK (AF6423, 1:1000, Affinity), anti-p-AMPK (AF3423, 1:1000, Affinity), PEPCK (DF6770, 1:1000, Affinity), G6P (DF6444, 1:1000, Affinity), and anti-GAPDH(AF7021, 1:3000, Affinity). After washing, the membranes were blotted with secondary antibodies (1:10,000, dilute with antibody diluent) for 1 h at room temperature, followed by detection using an electrogenerated chemiluminescence (ECL) system.

Glycogen Content Assay

The glycogen content of the HepG2 cells was determined using a glycogen assay kit from Nanjing Jiancheng Bioengineering Institute (Nanjing, China). The wavelength of the blue compound generated by the reaction was 620 nm.

Small Interferon RNA (siRNA) Knockdown

HepG2 cells were transfected with a negative control siRNA or si-PI3K (GenePharma, Suzhou, China). HepG2 cells were transfected with a final concentration of 100 nM siRNA for 72 h, and transfection efficiency was determined by Western blotting.

HOMA-IR

HOMA-IR was used to evaluate the level of insulin resistance in individuals.[28] The calculation method is as follows: fasting blood glucose level (FPG, mmol/L) × fasting insulin level (FINS, μU/mL) /22.5, HOMA-IR index of normal individuals is 1. As the level of insulin resistance increases, the HOMA-IR index will be higher than 1.

2-NBDG Uptake Assay

HepG2 cells were seeded in 24-well plates, the culture medium was discarded and trypsin was added to digest cells. After the supernatant was discarded by centrifugation, the supernatant was washed twice with PBS, and 1 mL 2-NBDG working liquid was added (2.92 mL DDH2O diluted 1 mg 2-NBDG to prepare 1 mM reserve liquid), incubated at room temperature for 30 minutes, 3400 g, centrifuged at 4°C for 3 to 3 minutes, and the supernatant was discarded. PBS was added to wash the cells twice. After the cells were suspended with 1 mL serum-free medium or PBS, confocal microscopy was used to observe the cells.

Statistical Analysis

All experiments were repeated three times. All data are presented as mean ± standard deviation (SD). Statistical and graphical analyses were performed using GraphPad Prism 8.0 (GraphPad Software, USA). For comparison of the two groups, significance was assessed using Student's *t*-test. For multiple group comparisons, significance was assessed using one-way analysis ANOVA with Tukey's post-hoc test. $P < 0.05$ was statistically significant.

Results

Isolation and Identification of Mouse BMSCs

We isolated and characterized the BMSCs used in this study. Consistent with the International Society for Cell Therapy (ISCT) criteria,[29] the BMSCs showed a spindle shape (Figure 1A). In addition, the isolated BMSCs were undifferentiated, and Oil Red O, Alcian Blue, and Alizarin Red staining showed that BMSCs had lipogenic, chondrogenic, and osteogenic differentiation potentials after induction in lipogenic, chondrogenic, or osteogenic media (Figure 1A). It was confirmed that BMSCs have the characteristics of three-directional differentiation of stem cells. As shown in Supplementary Figure 1C, both H8 and H8NV exhibit a prominent peak at 1705 cm^{-1}, indicating the presenceof carbonyl (-C-O) derived from the cyclopentane unit structure in H8. Furthermore, twocharacteristic peaks observed at 1157 and 794 cm^{-1} correspond to C-H bending vibrations and further confirm the presence of -CH2 bonds. And, the stretching vibration bond of -C-C was observed at 1635 cm^{-1} and 1457 cm^{-1}, indicating the existence of unsaturated carbon bonds, which originate from the structural framework of H8's benzene unit. These Results indicate that H8 is successfully encapsulated in vesicles.

Preparation and Characterization of H8-BMSCs-NVs

To determine the optimal concentration of H8 for BMSCs, they were treated with different concentrations of H8 for 24 and 48 h. There was no significant difference between the results at 24 and 48 h by MTT analysis (Figure 1B and C). The survival rate of BMSCs was still high at the concentration of H8 of 15 μM (Figure 1B–F). An H8 concentration of 15 μM was selected for the subsequent experiments. We isolated NVs from BMSCs by using a microvesicle extruder. BMSCs, BMSCs-NVS and H8-BMSCs-NVs markers were identified by Western blot analysis. The BMSCs protein markers CD9

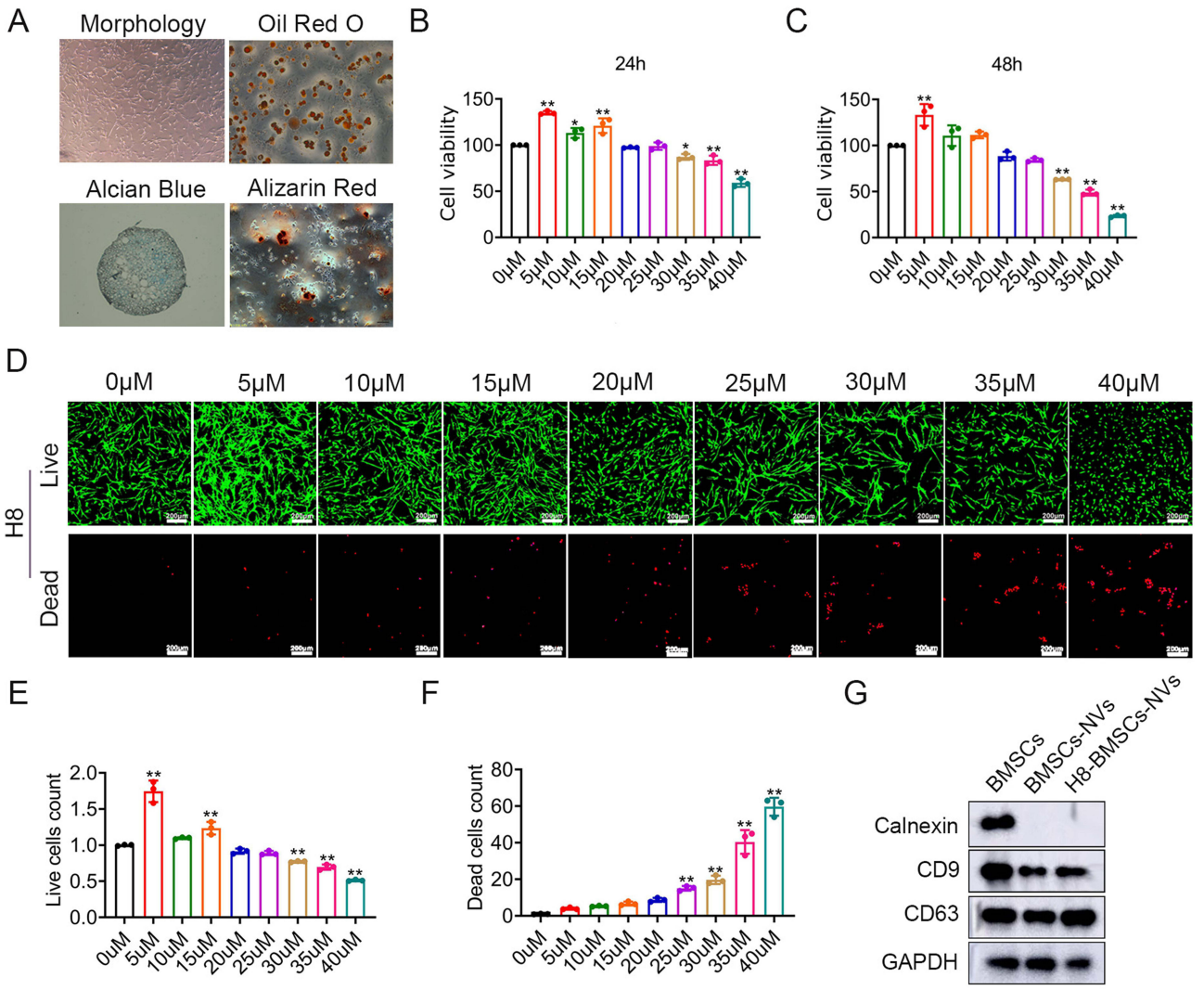

Figure 1 Preparation and identification of H8-BMSCs-NVs. (**A**) Morphology and three-way induced differentiation of BMSCs. (**B**–**F**) BMSCs were treated with different concentrations of H8. BMSCs Cell viability at 24 h (**B**) and 48 h (**C**). (**D**) Representative images of live and dead cells. Proportion of live (**E**) and dead (**F**) cells. (**G**) Western blotting showing characteristics of BMSCs and NVs using the BMSC markers, CD9 and CD63, and the endoplasmic reticulum marker, calnexin. (*P<0.05, **P<0.01 vs control).

and CD63 were enriched in MSCs, while calnexin, an endoplasmic reticulum marker, was present in cells but absent in NVs (Figure 1G). These data confirmed the successful preparation of H8-BMSCs-NVs.

H8-BMSCs-NVs Improved Glucose Tolerance and Increased Insulin Sensitivity in T2D Mice

To test the hypoglycemic effect of H8-BMSCs-NVs in vivo, we established an HFD/STZ-induced T2D mouse model. A significant increase in body weight and blood glucose levels confirmed the successful construction of the T2D model (Supplemental Figure 1A, B, 2A and B). After treatment with H8-BMSCs-NVs, BMSCs-NVs, and H8, the weight of T2D mice decreased significantly. The effect of H8-BMSCs-NVs was the most prominent, and the weight of T2D mice returned to normal after 8 weeks of treatment (Figure 2A). Meanwhile, H8-BMSCs-NVs were the most effective in reducing blood glucose levels in T2D mice (Figure 2B). The results of the IPGTT (Figure 2C and D) and IPITT (Figure 2E and F) revealed that H8-BMSCs-NVs significantly ameliorated glucose metabolism and insulin sensitivity in T2D mice. In addition, we measured serum glucose and insulin levels after eight weeks of treatment with H8-BMSCs-NVs, BMSCs-NVs, and H8. H8-BMSCs-NVs most significantly reduced serum glucose and insulin levels compared to the other groups (Figure 2G and H).

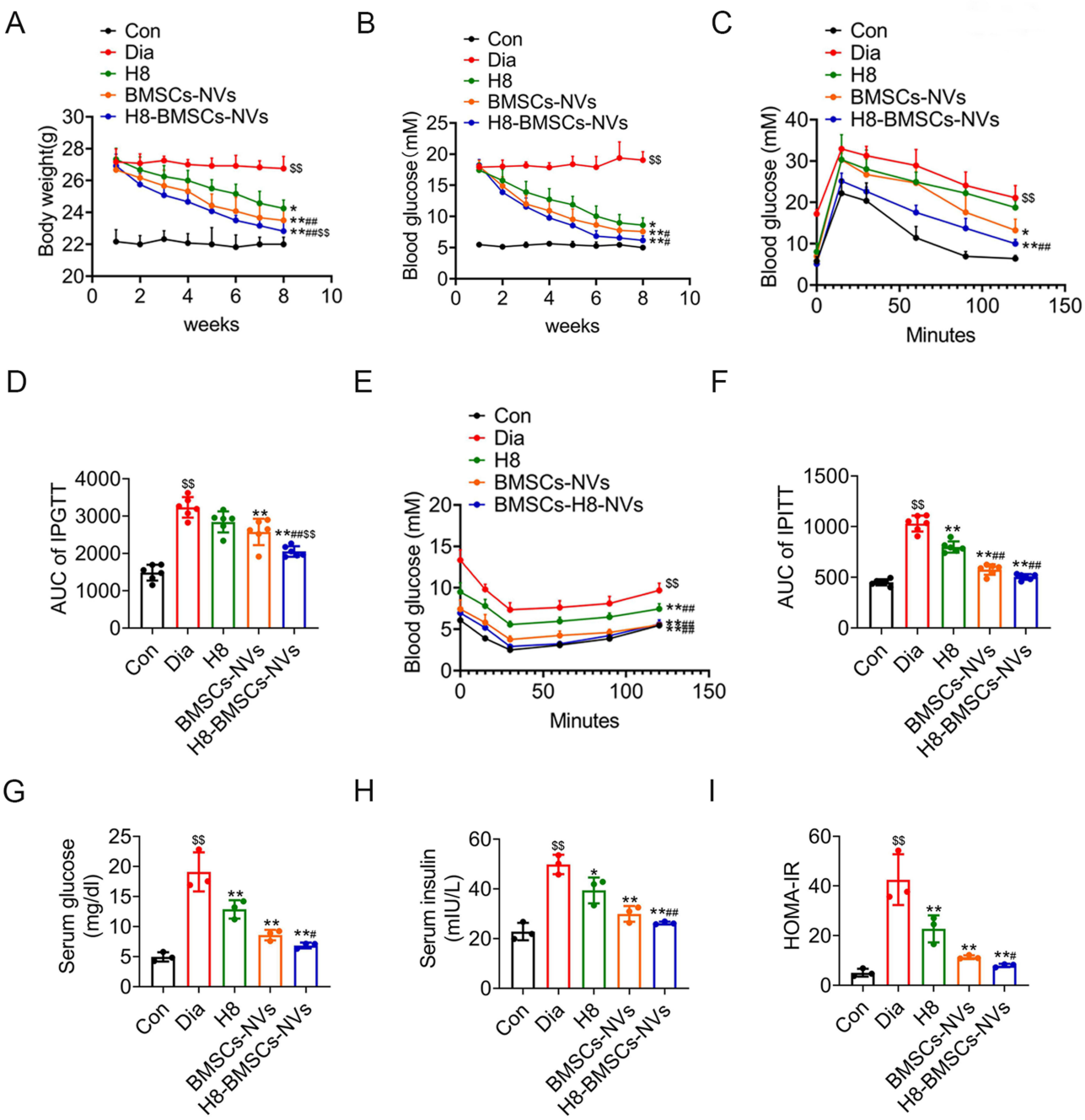

Figure 2 H8-BMSCs-NVs improve glucose tolerance and increase insulin sensitivity in T2D mice. C57BL/6J male mice were induced T2D by HFD/STZ and treated with H8, BMSCs-NVs and H8-BMSCs-NVs for 8 weeks. (**A**) Changes in body weight were monitored during the experiment. (**B**) Blood glucose levels measured during the experiment. (**C** and **D**) Results of IPGTT and the corresponding AUC. (**E** and **F**) Results of the IPITT assay and the corresponding AUC. Serum glucose level (**G**), serum insulin level (**H**) and HOMA-IR index (**I**) when mice were harvested. All results are expressed as mean ± SD (n = 6 mice per group, $^{\$}$$P<0.01, vs control, *P<0.05, **P<0.01, vs Dia, $^{\#}$P<0.05, $^{\#\#}$P<0.01, vs H8).

Homeostasis model of insulin resistance (HOMA-IR) is commonly used to quantify insulin resistance. H8-BMSCs-NVs also most significantly decreased the HOMA-IR index compared with the other groups (Figure 2I). These data suggest that H8-BMSCs-NVs improved glucose tolerance and increase insulin sensitivity in T2D mice.

H8-BMSCs-NVs Relieved Liver Dysfunction and Improved Lipid Profiles in T2D Mice

We further verified the effects of the H8-BMSCs-NVs on liver dysfunction and lipid metabolism. Treatment with H8, BMSC-NVs, and H8-BMSCs-NVS significantly alleviated the increase in hepatic steatosis and liver weight in T2D mice (Figure 3A and

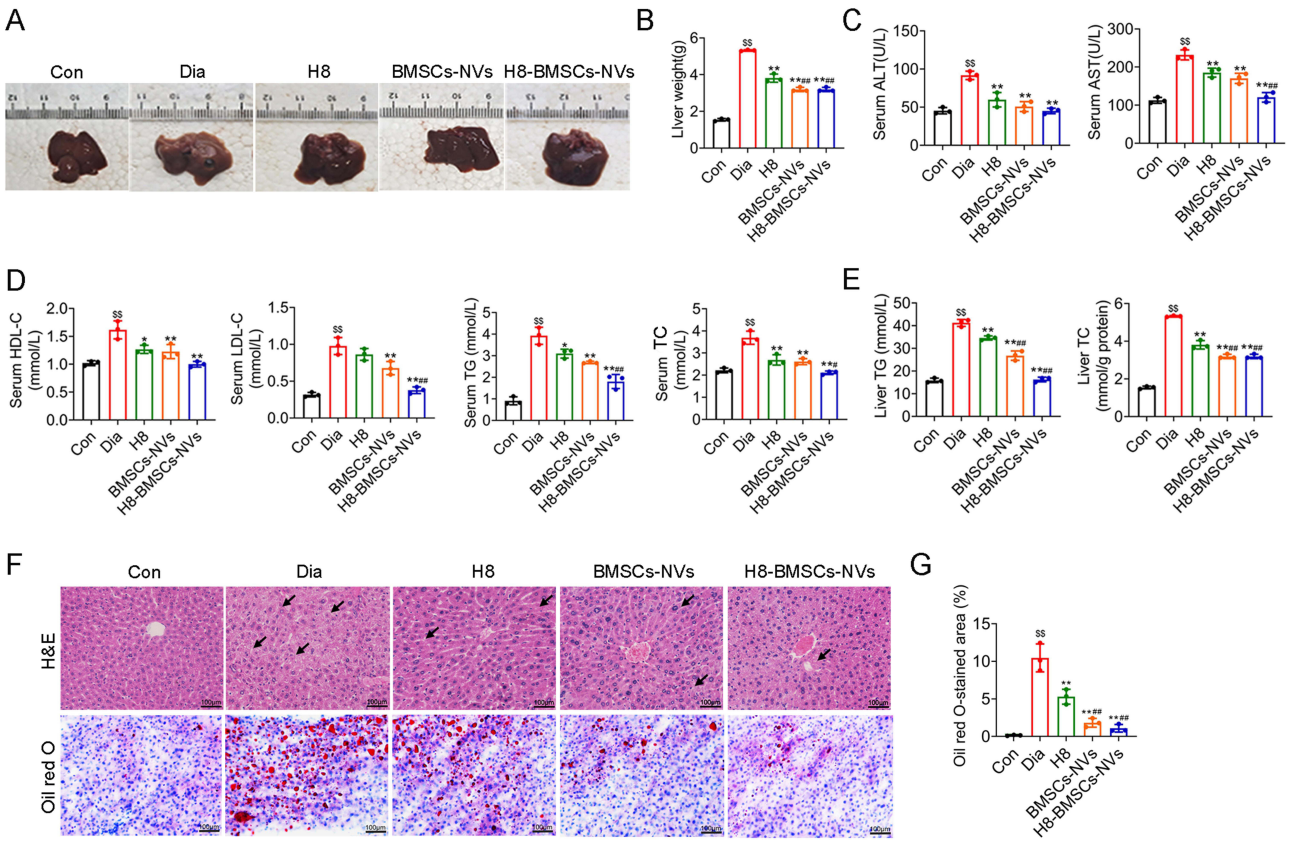

Figure 3 H8-BMSCs-NVs improved liver dysfunction and reduced lipid levels in T2D mice. C57BL/6J male mice were induced T2D by HFD/STZ and treated with H8, BMSCs-NVs and H8-BMSCs-NVs for 8 weeks. (**A** and **B**) Macroscopic photographs of the liver and liver weights. (**C**) Serum ALT and AST levels. (**D**) Serum HDL-C, LDL-C, TG, and TC levels. (**E**) Liver TG and TC levels. (**F**) H&E and Oil Red O staining of liver sections from different mouse groups (scale bar, 100 μm). (**G**) Quantitative analysis of oil red O staining. All results are expressed as mean ± SD (n = 6 mice per group, $$P<0.01, vs control, *P<0.05, **P<0.01, vs Dia, #P<0.05, ##P<0.01, vs H8).

B). ALT and AST, which are important indicators of liver dysfunction, were significantly elevated in T2D mice compared to those in the control group, while the levels of ALT and AST in H8, BMSCs-NVs and H8-BMSCs-NVs-treated groups were significantly decreased, and the therapeutic effect of H8-BMSCs-NVs was the most significant (Figure 3C). In addition, we found that H8-BMSCs-NVs most effectively promoted lipid metabolism by analyzing the serum lipid profiles (HDL-C, LDL-C, TG, and TC) (Figure 3D) and liver lipid profiles (TG and TC) (Figure 3E). The results of liver tissue H&E and Oil Red O staining analysis showed that H8-BMSCs-NVs significantly alleviated liver dysfunction and improved lipid accumulation in T2D mice (Figure 3F and G). We found that H8-BMSCs-NVs also had the effect of alleviating fibrosis by Masson and Sirius red staining (Supplementary Figure 2). These data suggest that H8-BMSCs-NVs improved liver dysfunction and lipid profiles in T2D mice.

H8-BMSCs-NVs Alleviated Inflammatory Response in T2D Mice

We detected the expression levels of inflammatory factors in the serum and liver tissues using ELISA kits, and the experimental results showed that H8-BMSCs-NVs most significantly decreased the expression of pro-inflammatory factors (IL-6, IL-1β, and TNF-α) and increased the expression of anti-inflammatory factors (IL-10 and IL-11) in T2D mice (Figure 4A and B). To further ascertain the tissue toxicities of H8-BMSCs-NVs, histochemical analysis of the heart, liver, spleen, lung, kidney, and brain was conducted after administration. No apparent evidence of damage or abnormality was detected in H&E-stained sections of major organs harvested from BMSC-NVs or H8-BMSC-NVs -treated mice (Supplementary Figure 3). These data suggested that H8-BMSC-NVs inhibited the inflammatory response in T2D mice.

H8-BMSCs-NVs Improve Glucose and Lipid Metabolism in vitro

To investigate the mechanism of H8-BMSCs-NVs against insulin resistant, the corresponding cell line (HepG2) was used to investigate. First, we examined the effects of BMSCs-NVs and H8-BMSCs-NVs at different concentrations of and

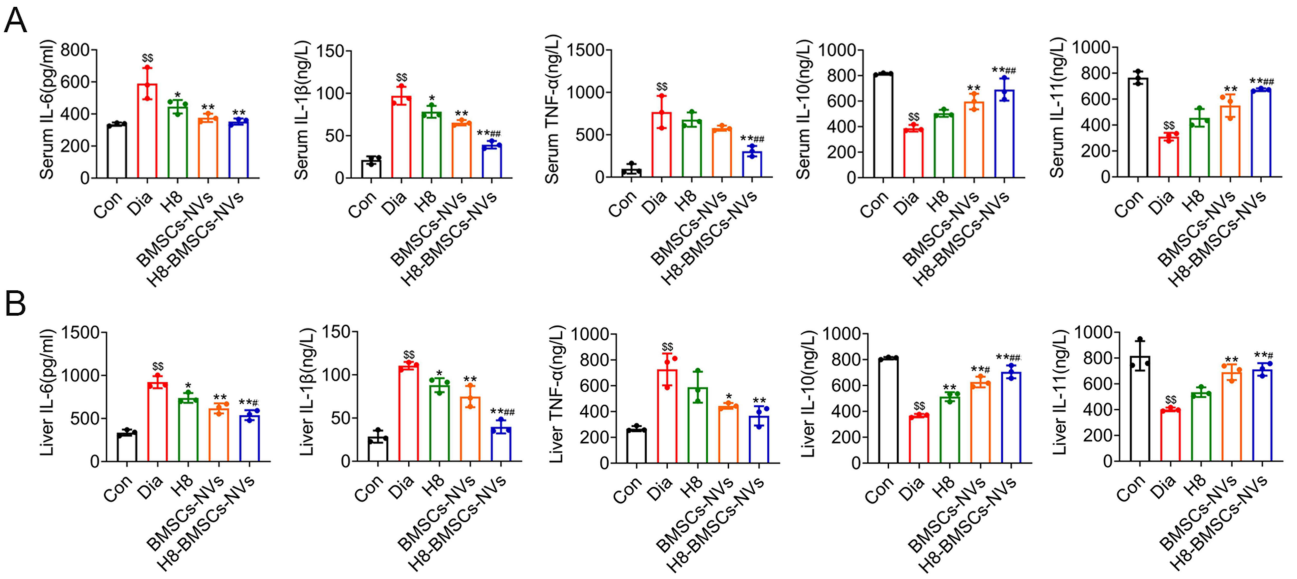

Figure 4 H8-BMSCs-NVs improved inflammatory response in T2D mice. C57BL/6J male mice were induced T2D by HFD/STZ and treated with H8, BMSCs-NVs and H8-BMSCs-NVs for 8 weeks. (**A**) Serum levels of IL-6, IL-1β, TNF-α, IL-10, and IL-11 were quantified by ELISA kits. (**B**) Liver levels of IL-6, IL-1β, TNF-α, IL-10, and IL-11 were quantified using ELISA kits. All results are expressed as mean ± SD (n = 6 mice per group, $^{\$\$}$P<0.01, vs control, *P<0.05, **P<0.01, vs Dia, $^{\#}$P<0.05, $^{\#\#}$P<0.01, vs H8).

viability on HepG2 cell viability. We found that both 5 μg/mL BMSCs-NVs and H8-BMSCs-NVs significantly increased cell viability, with the highest efficiency at 15 μg/mL and toxicity at concentrations above 30 μg/mL (Figure 5A and B). Therefore, BMSCs-NVs and H8-BMSCs-NVs at 5, 10, and 30 μg/mL were selected for further analyses.

An insulin-resistant HepG2 cell model was established as previously described.[30] As shown in Figure 5C and D, the expression levels of TG and TC were significantly increased in the high glucose and high insulin (HGHI) groups compared to the control group. Treatment with BMSCs-NVs and H8-BMSCs-NVs reduced the TG and TC levels induced by the insulin resistance model. We found that the treatment effect of H8-BMSCs-NVs was better than that of BMSC-NVs in a dose-dependent manner, with the best treatment effect observed at a concentration of 30 μg/mL. Hence, H8-BMSCs-NVs at a concentration of 30 μg/mL were selected for subsequent experiments. The endocytosis assay showed that both BMSCs-NVs and H8-BMSCs-NVs were internalized by HepG2 cells (Figure 5E).

Glucose consumption in the HGHI group decreased significantly (Figure 5F–J), indicating that an extra amount of insulin was unable to exert its function and even caused hyperglycemia and impaired glucose metabolism in insulin-responsive cells. However, treatment with H8, BMSC-NVs, and H8-BMSCS-NVS increased glucose uptake and reduced lipid accumulation in HepG2 cells, with the most significant effect observed for H8-BMSCS-NVS (Figure 5F–H). Similarly, H8-BMSCs-NVs most significantly increased glucose consumption and glycogen content under HGHI conditions (Figure 5I and J).

H8-BMSCs-NVs Improve Glucose and Lipid Metabolism by PI3K/AKT/AMPK Signaling Pathway

The PI3K/AKT/AMPK signaling pathway is a critical regulator of T2D,[31] and its activation leads to suppression of gluconeogenesis and enhancement of glycogen synthesis.[32] Western blot analysis showed that the expression levels of p-PI3K, p-AKT, and p-AMPK in the liver tissues of T2D mice were significantly decreased (Figure 6A and B). In addition, the expression levels of two key liver gluconeogenic enzymes, PEPCK and G6P, significantly increased in the liver tissues of T2D mice (Figure 6A and B). Treatment with H8, BMSCs-NVs and H8-BMSCs-NVs significantly activated the PI3K/AKT/AMPK signaling pathway and decreased the expression of PEPCK and G6P, among which H8-BMSCs-NVs showed the most significant therapeutic effect (Figure 6A and B). This process was verified in vitro. Consistent with the results of the animal experiments, the treatment effect of H8-BMSCs-NVs was most significant under HGHI conditions (Figure 6C and D).

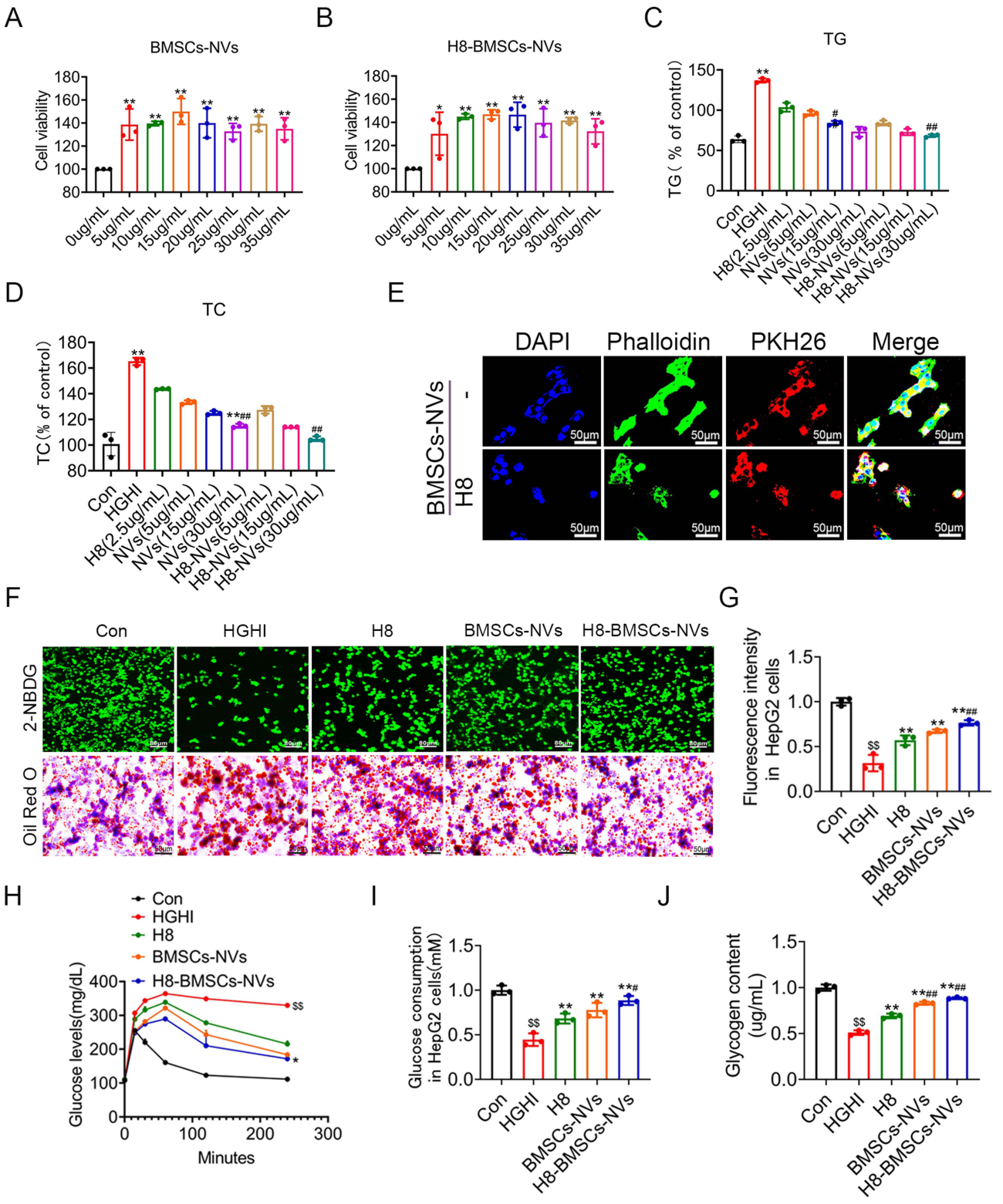

Figure 5 H8-BMSCs-NVs decreased glucose consumption and uptake in HGHI-induced insulin-resistant HepG2 cells. (**A**) HepG2 cells were incubated with various concentrations of BMSC-NVs for 24 hours. Cell viability was determined using an MTT assay. (**B**) HepG2 cells were incubated with different concentrations of the H8-BMSCs-NVs for 24 h. Cell viability was determined using an MTT assay. (**C** and **D**) TG and TC levels in different treatment groups were detected using biochemical kits. (**E**) Cellular uptake of NVs. (**F**) 2-NBDG uptake and Oil Red O staining of HepG2 cells. (**G**) Quantitative analysis of 2-NBDG uptake. Glucose levels (**H**), glucose consumption (**I**), and glycogen content (**J**) in different treatment groups were determined using biochemical kits. Data are representative of at least three independent experiments ($ $P<0.01 vs control, *P<0.05, **P<0.01, vs HGHI; # P<0.05, ## P<0.01, vs H8).

To further analyze whether H8-BMSCs-NVs regulate PEPCK and G6P expression through the PI3K/AKT/AMPK signaling pathway, we performed molecular mechanistic studies using a PI3K inhibitor (LY294002) and siRNA (si-PI3K) . LY294002 significantly inhibited the H8-BMSCs-NVs activation of the PI3K/AKT/AMPK signaling pathway and restored the H8-BMSCs-NVs reduced PEPCK and G6P under HGHI conditions (Figure 7A and B). The experimental results for si-PI3K and LY294002 were consistent (Figure 7C and D). These data suggested that H8-BMSCs-NVs inhibited the expression of PEPCK and G6P by activating the PI3K/AKT/AMPK signaling pathway.

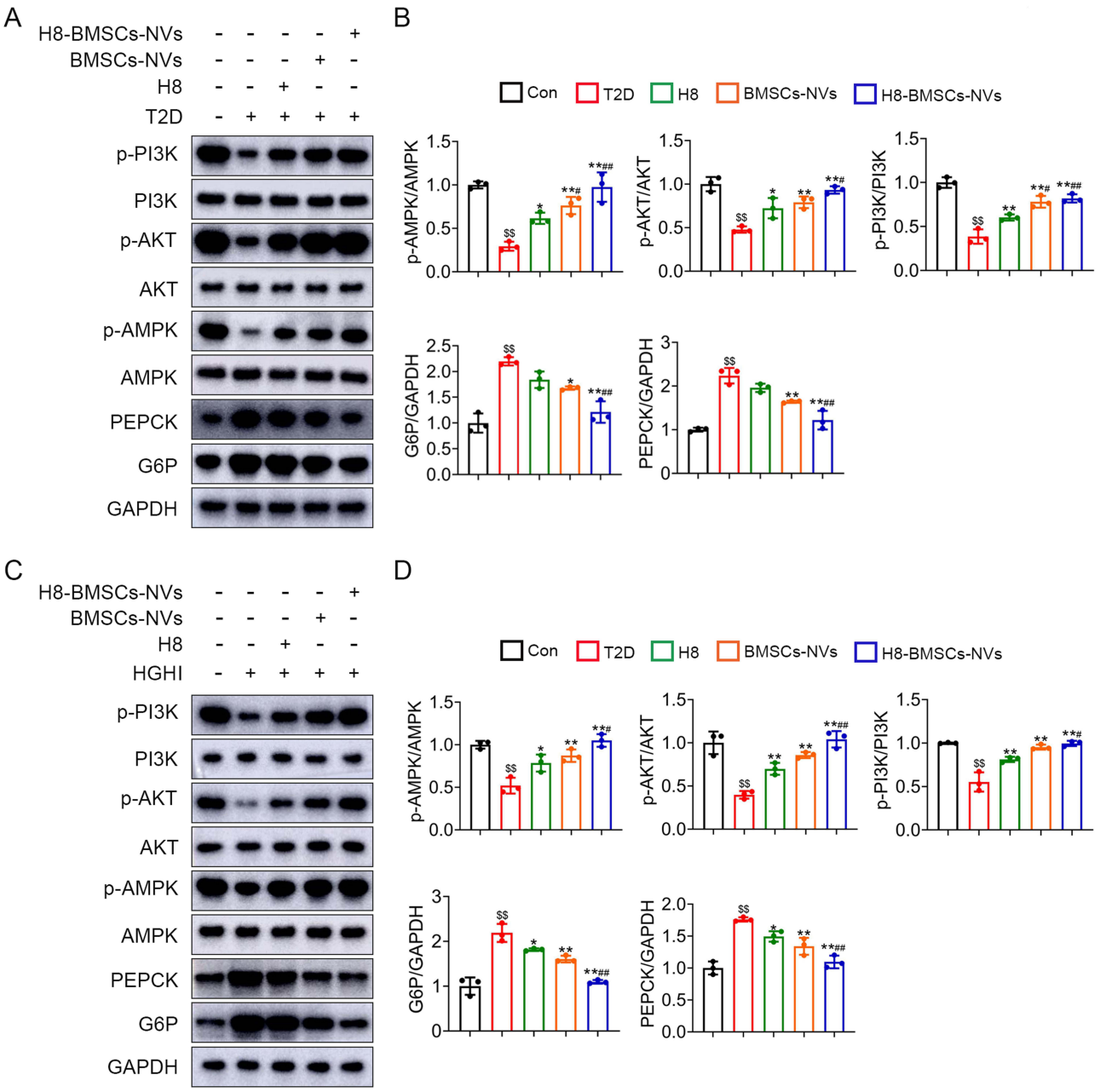

Figure 6 H8-BMSCs-NVs activated the PI3K/AKT/AMPK signaling pathway and reduced the expression levels of G6P and PEPCK. (**A** and **B**) C57BL/6J male mice were induced T2D by HFD/STZ and treated with H8, BMSCs-NVs and H8-BMSCs-NVs for 8 weeks. The expression levels of p-PI3K, PI3K, p-AKT, AKT, p-AMPK, AMPK, PEPCK, and G6P proteins in liver tissues were determined using Western blot analysis. Protein density was quantified by densitometry. Phosphoprotein levels were normalized to total protein levels. The PEPCK and G6P levels were normalized to those of GAPDH. Data are representative of at least three independent experiments ($^{\$\$}$P<0.01 vs control, *P<0.05, **P<0.01 vs T2D, $^{\#}$P<0.05, $^{\#\#}$P<0.01 vs H8). (**C** and **D**) HepG2 cells were incubated with H8, BMSCs-NVs or H8-BMSCs-NVs for 24 h. The expression levels of p-PI3K, PI3K, p-AKT, AKT, p-AMPK, AMPK, PEPCK and G6P proteins in HepG2 cells were determined using Western blot analysis. The densities of proteins were quantified using densitometry. Phospho-proteins were normalized to total proteins. PEPCK and G6P were normalized to GAPDH. The data are representative of at least three independent experiments ($$P<0.01, vs control; *P<0.05, **P<0.01 vs HGHI; $^{\#}$P<0.05, $^{\#\#}$P<0.01, vs H8).

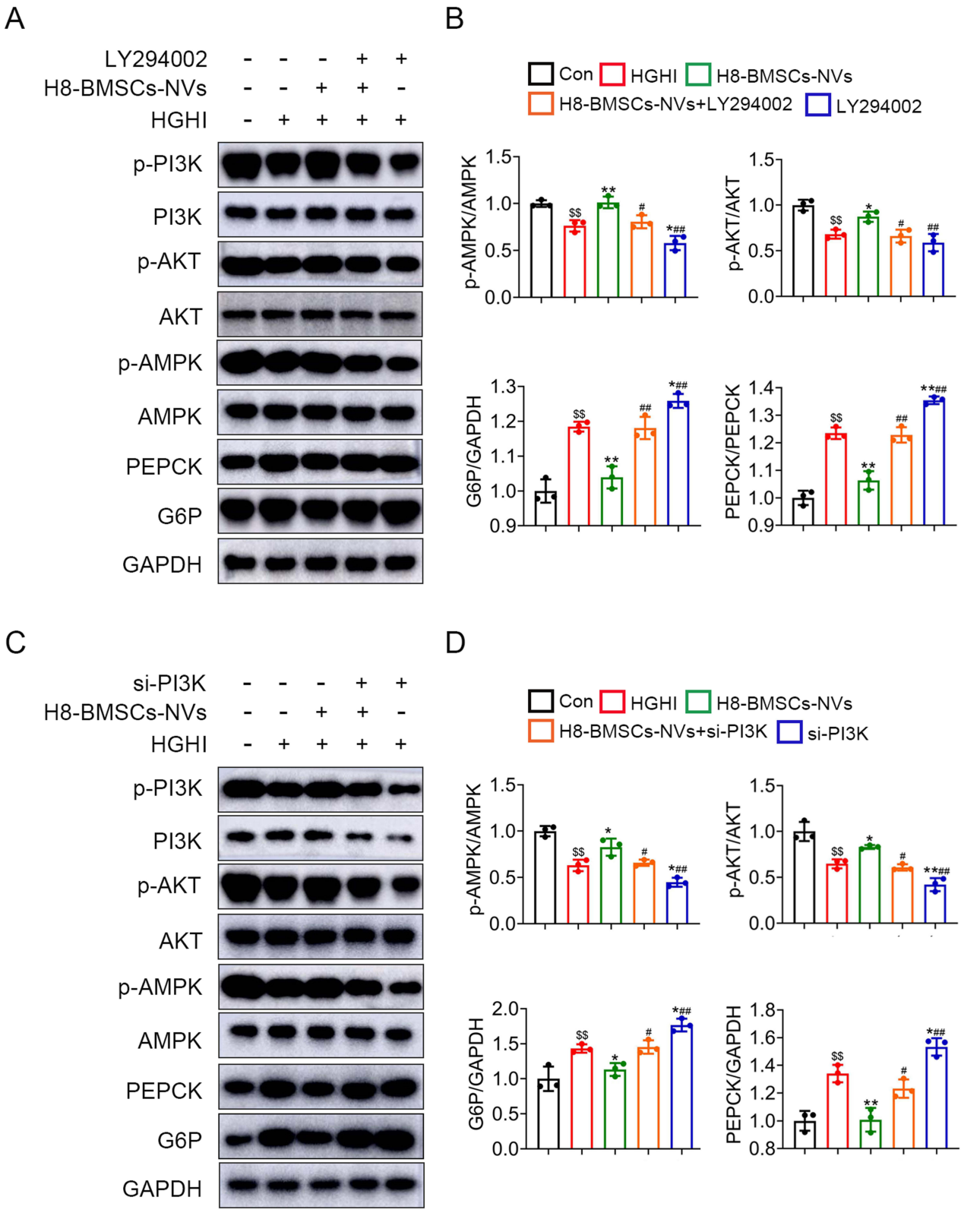

Figure 7 H8-BMSCs-NVs decreased G6P and PEPCK expression by the PI3K/AKT/AMPK signaling pathway. (**A** and **B**) HepG2 cells were incubated with H8-BMSCs-NVs or LY294002 for 24 h. The expression levels of p-PI3K, PI3K, p-AKT, AKT, p-AMPK, AMPK, PEPCK, and G6P proteins in HepG2 cells were determined using Western blot analysis. (**C** and **D**) HepG2 cells were incubated with H8-BMSCs-NVs or si-PI3K for 24 h. The expression levels of p-PI3K, PI3K, p-AKT, AKT, p-AMPK, AMPK, PEPCK, and G6P proteins in HepG2 cells were determined using Western blot analysis. Protein density was quantified by densitometry. Phosphoprotein levels were normalized to total protein levels. The PEPCK and G6P levels were normalized to those of GAPDH. The data are representative of at least three independent experiments ($^{\$\$}$P<0.01 vs control, *P<0.05, **P<0.01 vs HGHI, $^{\#}$P<0.05, $^{\#\#}$P<0.01 vs H8-BMSCs-NVs).

In order to verify whether PI3K inhibitor has the same effect in vivo, we measured the serum TC, TG, HDL-C and LDL-C contents after intraperitoneally injecting PI3K inhibitor into mice in the H8-BMSCs-NVs group. We found that the effects of H8-BMSCs-NVS on liver function in mice with type 2 diabetes were largely reversed by inhibitors (Supplementary Figure 4).

Discussion

NVs are tiny nanoparticles that can carry drugs to specific cells or tissues, with the advantage of precision therapy. In this study, we confirmed that H8-BMSCs-NVs reduced blood glucose levels, effectively alleviated liver steatosis, and restored liver function in T2D mice. In addition, we confirmed that H8-BMSCs-NVs effectively inhibited lipid accumulation in HepG2 cells in an insulin-resistant model. Mechanistic analysis, H8-BMSCs-NVs inhibited the expression levels of G6P and PEPCK by activating the PI3K /AKT/AMPK signaling pathway.

Extracellular vesicles have been extensively studied as small membrane-bound vesicles released by cells into the extracellular environment.[33] They contain a range of biomolecules, including proteins, nucleic acids, and lipids, which typically range in diameter from 30–150 nanometres and are able to cross biological barriers such as the blood-brain barrier, making them promising vectors for drug delivery and disease diagnosis.[34] The unique composition and biocompatibility of NVs make it an attractive candidate for drug delivery systems and regenerative medicine. NVs play an important role in intercellular communication, allowing cells to exchange information and materials.[35] One of the most promising applications of NVs is drug delivery. Because they are naturally produced by cells, NVs are non-toxic and biocompatible.

NVs is an adaptable and promising drug transport and targeting system.[36,37] Compared to other microstructures, NVs have both hydrophilic and hydrophobic microregions, which enable them to deliver both water-soluble and lipid-soluble drugs.[38,39] NVs are ideal drug carriers in vivo because of their biofilm structure and good biocompatibility with biofilm.[40] In recent years, several studies have demonstrated the use of NVs as diabetes drug delivery systems to reduce glucose and improve insulin sensitivity.[22,23] In the present study, we prepared biomimetic exosome NVs generated by continuous extrusion with a microvesicle extruder. These vesicles are similar to exosomes in terms of size, morphology, and function, and have the advantages of high yield and a simple preparation process.

In previous studies, we found that H8 reduced the effect of reducing blood glucose concentration and effectively improved insulin sensitivity in T2D mice, and the effect was better than that of curcumin.[41,42] In this study, NVs were used as a sustained-release agent to encapsulate H8, and more biologically targeted nanodrugs (H8-BMSCS-NVS) were prepared by taking advantage of the fact that it takes a long time for molecules to enter and exit the NVs. Our results demonstrated that H8-BMSCs-NVs effectively improved insulin resistance, inhibited hepatic steatosis, and restored impaired liver function in T2D mice. H8-BMSCs-NVs also effectively reduced TG and TC levels and inhibited intracellular lipid accumulation in the insulin resistance model. However, our current studies are limited to mouse and cellular models, and further validation is required in T2D patients.

However, how H8-BMSCs-NVs regulates the immune component, how long it can act in the body after administration, and whether long-term use will produce biological toxicity are the limitations of our study.

The PI3K/AKT/AMPK signaling pathway plays a key role in glucose homeostasis and energy metabolism, and is a potential therapeutic target for T2D.[43,44] Binding of insulin to its receptor activates the PI3K/AKT signaling pathway, leading to the translocation of GLUT4 to the cell membrane and promoting glucose uptake.[45] In an insulin resistance model, activation of the PI3K/AKT signaling pathway led to reduced glucose uptake and utilization.[46] AMPK phosphorylation promotes glucose uptake and utilization in muscles and inhibits glucose production in the liver.[47] G6P and PEPCK are important regulatory enzymes in the glucose metabolic pathway, and are essential for maintaining blood glucose levels during fasting or glucose requirements.[48] In this study, we found that H8-BMSCs-NVs significantly activated the PI3K/AKT/AMPK signaling pathway and further inhibited the expression levels of G6P and PEPCK in the HepG2 cell insulin resistance and T2D mouse models. According to research, Nuclear FoxO1 and its downstream genes PEECK and G6P were decreased in the livers of the lipocalin2 (LCN2) knockout (LCN2KO) mice, and AMPK activity was stimulated and directly phosphorylated FoxO1.[49] In vitro, AMPK activity was inhibited in HepG2 cells overexpressing LCN2 leading to a decrease in

phosphorylated FoxO1 and an increase in nuclear FoxO1. However, the upstream and downstream relationships of proteins in this signaling pathway need to be further explored. Also, we think that primary hepatocytes may be better at replicating in vivo conditions, which is a limitation of our experiment. Studies have shown that, Application of curcumin-loaded permeation enhancer nanovesicles (PE-NVs) reduced symptoms of hyperpigmentation because of higher accumulation because of better permeation into skin layers. Results confirmed that PE-NVs is a potential drug delivery system for topical administration drugs to treat skin-associated inflammatory disorders.[50] Previous studies have also found that H8-BMSCS-NVS also has a good therapeutic effect on diabetic wounds, inhibits inflammation and promotes angiogenesis.[51] Therefore, the mechanism of H8-BMSCs-NVs is still worth further exploration.

In conclusion, our study confirmed that H8-BMSCs-NVs regulated lipid metabolism disorders and played a hypoglycemic role by activating the PI3K/AKT/AMPK signaling pathway, thus improving insulin resistance in T2D mice. This study provides a new research basis for the treatment of T2D.

Conclusion

In Conclusion, we have successfully prepared H8-BMSCs-NVs. It can improve glucose tolerance, increase insulin sensitivity, improve liver dysfunction, inflammatory response and reduced lipid levels in T2D mice. Meanwhile, H8-BMSCs-NVs effectively inhibited intracellular lipid accumulation in insulin resistance models of HepG2 cells. Mechanism studies showed that H8-BMSCs-NVs activated the PI3K/AKT/AMPK signaling pathway and decreased the expression levels of G6P and PEPCK. Given the abilities of their therapy abilities, as well as the remarkable combined effectiveness and biosafety, H8-BMSCs-NVs might be a potential candidate to improve the treatment result of T2D, especially liver dysfunction. Due to the complex regulation of immune mechanism in vivo, how drugs regulate immune components needs further study. At the same time, we can only prove that the drug has a short-term effect in the body is safe, but in the long run, whether the drug has a certain biological toxicity we do not know. All these need our further Discussion.

Abbreviations

NVs, nanovesicles; H8-BMSCs-NVs, BMSCs-derived NVs carrying curcumin analogs H8; T2D, type 2 diabetes; NVs, nanovesicles; HFD, high-fat diet; STZ, streptozotocin; PA, palmitic acid; OA, oleic acid; DMSO, dimethyl sulfoxide; IPGTT, Intraperitoneal glucose tolerance test; IPITT, intraperitoneal insulin tolerance test; H&E, hematoxylin and eosin; ELISA, enzyme-linked immunosorbent assay; IL-6, interleukin-6; ALT, Alanine aminotransferase; AST, aspartate aminotransferase; HDL-C, high-density lipoprotein cholesterol; LDL-C, low-density lipoprotein cholesterol; TG, triglyceride; TC, total cholesterol; BCA, bicinchoninic acid; ECL, electrogenerated chemiluminescence; SD, standard deviation; ISCT, International Society for Cell Therapy; HOMA-IR, Homeostasis model of insulin resistance; HGHI, high glucose and high insulin.

Acknowledgments

This research was supported by funding from the Torch Program of the Mudanjiang Medical College Science Foundation (2022-MYHJ-006) and National Natural Science Foundation of Heilongjiang Province (LH2023H053).

Disclosure

The authors declare that they have no conflicts of interest.

References

1. Gregg EW, Buckley J, Ali MK, et al. Improving health outcomes of people with diabetes: target setting for the WHO Global Diabetes Compact. *Lancet*. 2023. doi:10.1016/s0140-6736(23)00001-6
2. Zheng Y, Ley SH, Fb HU. Global aetiology and epidemiology of type 2 diabetes mellitus and its complications. *Nat Rev Endocrinol*. 2018;14(2):88–98. doi:10.1038/nrendo.2017.151
3. Ling C, Rönn T. Epigenetics in human obesity and type 2 diabetes. *Cell Metab*. 2019;29(5):1028–1044. doi:10.1016/j.cmet.2019.03.009

4. Saeedi P, Petersohn I, Salpea P, et al. Global and regional diabetes prevalence estimates for 2019 and projections for 2030 and 2045: results from the International Diabetes Federation Diabetes Atlas, 9(th) edition. *Diabet Res Clin Pract*. 2019;157:107843. doi:10.1016/j.diabres.2019.107843
5. Daly A, Hovorka R. Technology in the management of type 2 diabetes: present status and future prospects. *Diabetes Obes Metab*. 2021;23 (8):1722–1732. doi:10.1111/dom.14418
6. Ahmad E, Lim S, Lamptey R, et al. Type 2 diabetes. *Lancet*. 2022;400(10365):1803–1820. doi:10.1016/s0140-6736(22)01655-5
7. Huang Z, Wan X, Liu J, et al. Short-term continuous subcutaneous insulin infusion combined with insulin sensitizers rosiglitazone, metformin, or antioxidant α-lipoic acid in patients with newly diagnosed type 2 diabetes mellitus. *Diabetes Technol Ther*. 2013;15(10):859–869. doi:10.1089/dia.2013.0013
8. Weng W, Goel A. Curcumin and colorectal cancer: an update and current perspective on this natural medicine. *Semin Cancer Biol*. 2022;80:73–86. doi:10.1016/j.semcancer.2020.02.011
9. Tossetta G, Fantone S, Giannubilo SR, et al. The multifaced actions of curcumin in pregnancy outcome. *Antioxidants*. 2021;10(1). doi:10.3390/antiox10010126
10. Chen Y, Lu Y, J LR, et al. Nano encapsulated curcumin: and its potential for biomedical applications. *Int J Nanomed*. 2020;15:3099–3120. doi:10.2147/ijn.S210320
11. Hajavi J, Momtazi AA, Johnston TP, et al. Curcumin: a naturally occurring modulator of adipokines in diabetes. *J Cell Biochem*. 2017;118 (12):4170–4182. doi:10.1002/jcb.26121
12. Altobelli E, Angeletti PM, Marziliano C, et al. Potential therapeutic effects of curcumin on glycemic and lipid profile in uncomplicated type 2 diabetes-a meta-analysis of randomized controlled trial. *Nutrients*. 2021;13(2). doi:10.3390/nu13020404
13. Panahi Y, Khalili N, Sahebi E, et al. Antioxidant effects of curcuminoids in patients with type 2 diabetes mellitus: a randomized controlled trial. *Inflammopharmacology*. 2017;25(1):25–31. doi:10.1007/s10787-016-0301-4
14. Duan X, Xin H, Yan H. Design, synthesis, and biological evaluation of 1,4-diaryl-1,4-dihydropyrazines as novel 11β-HSD1 inhibitors. *Biol Pharm Bull*. 2014;37(5):840–846. doi:10.1248/bpb.b14-00070
15. Yuan X, Li H, Bai H, et al. The 11β-hydroxysteroid dehydrogenase type 1 inhibitor protects against the insulin resistance and hepatic steatosis in db/db mice. *Eur J Pharmacol*. 2016;788:140–151. doi:10.1016/j.ejphar.2016.05.034
16. Galipeau J, Sensébé L. Mesenchymal stromal cells: clinical challenges and therapeutic opportunities. *Cell Stem Cell*. 2018;22(6):824–833. doi:10.1016/j.stem.2018.05.004
17. Qiu G, Zheng G, Ge M, et al. Functional proteins of mesenchymal stem cell-derived extracellular vesicles. *Stem Cell Res Ther*. 2019;10(1):359. doi:10.1186/s13287-019-1484-6
18. Fan L, Guan P, Xiao C, et al. Exosome-functionalized polyetheretherketone-based implant with immunomodulatory property for enhancing osseointegration. *Bioact Mater*. 2021;6(9):2754–2766. doi:10.1016/j.bioactmat.2021.02.005
19. Hu M, Zhang J, Kong L, et al. Immunogenic hybrid nanovesicles of liposomes and tumor-derived nanovesicles for cancer immunochemotherapy. *ACS Nano*. 2021;15(2):3123–3138. doi:10.1021/acsnano.0c09681
20. Ma W, Zhang X, Liu Y, et al. Polydopamine decorated microneedles with Fe-MSC-derived nanovesicles encapsulation for wound healing. *Adv Sci*. 2022;9(13):e2103317. doi:10.1002/advs.202103317
21. Xu Y, Zhang X, Zhang Y, et al. Mechanisms of deformable nanovesicles based on insulin-phospholipid complex for enhancing buccal delivery of insulin. *Int J Nanomed*. 2018;13:7319–7331. doi:10.2147/ijn.S175425
22. El-Marasy SA, Abousamra MM, El-Mosallamy A, et al. Chrysin loaded nanovesicles ameliorated diabetic peripheral neuropathy. Role of NGF/AKT/GSK-3β pathway. *Chem Biol Interact*. 2023;375:110402. doi:10.1016/j.cbi.2023.110402
23. Chen Q, Xiao Z, Wang C, et al. Microneedle patches loaded with nanovesicles for glucose transporter-mediated insulin delivery. *ACS Nano*. 2022;16(11):18223–18231. doi:10.1021/acsnano.2c05687
24. Liu Y, Li Z, Li J, et al. Stiffness-mediated mesenchymal stem cell fate decision in 3D-bioprinted hydrogels. *Burns Trauma*. 2020;8:tkaa029. doi:10.1093/burnst/tkaa029
25. Md Mokhtar AH, Malik IA, Abd Aziz NAA, et al. LY294002, a PI3K pathway inhibitor, prevents leptin-induced adverse effects on spermatozoa in Sprague-Dawley rats. *Andrologia*. 2019;51(3):e13196. doi:10.1111/and.13196
26. Marmentini C, Soares GM, Bronczek GA, et al. Aging reduces insulin clearance in mice. *Front Endocrinol*. 2021;12:679492. doi:10.3389/fendo.2021.679492
27. Pužar Dominkuš P, Stenovec M, Sitar S, et al. PKH26 labeling of extracellular vesicles: characterization and cellular internalization of contaminating PKH26 nanoparticles. *Biochim Biophys Acta Biomembr*. 2018;1860(6):1350–1361. doi:10.1016/j.bbamem.2018.03.013
28. Li D, Jiang C, Mei G, et al. Quercetin alleviates ferroptosis of pancreatic β cells in type 2 diabetes. *Nutrients*. 2020;12(10). doi:10.3390/nu12102954
29. Dominici M, Le Blanc K, Mueller I, et al. Minimal criteria for defining multipotent mesenchymal stromal cells. The International Society for Cellular Therapy position statement. *Cytotherapy*. 2006;8(4):315–317. doi:10.1080/14653240600855905
30. Zhang F, Hu Z, Li G, et al. Hepatic CREBZF couples insulin to lipogenesis by inhibiting insig activity and contributes to hepatic steatosis in diet-induced insulin-resistant mice. *Hepatology*. 2018;68(4):1361–1375. doi:10.1002/hep.29926
31. Wei ZZ, Weng YJ, Zhang YQ. Investigation of the repairing effect and mechanism of oral degraded sericin on liver injury in type II diabetic rats. *Biomolecules*. 2022;12(3). doi:10.3390/biom12030444
32. Ren Z, Xie Z, Cao D, et al. C-Phycocyanin inhibits hepatic gluconeogenesis and increases glycogen synthesis via activating Akt and AMPK in insulin resistance hepatocytes. *Food Funct*. 2018;9(5):2829–2839. doi:10.1039/c8fo00257f
33. Moghassemi S, Dadashzadeh A, Sousa MJ, et al. Extracellular vesicles in nanomedicine and regenerative medicine: a review over the last decade. *Bioact Mater*. 2024;36:126–156. doi:10.1016/j.bioactmat.2024.02.021
34. Luo H, Birjandi AA, Ren F, et al. Advances in oral mesenchymal stem cell-derived extracellular vesicles in health and disease. *Genes Dis*. 2024;11 (1):346–357. doi:10.1016/j.gendis.2023.03.015
35. Hu W, Wang W, Chen Z, et al. Engineered exosomes and composite biomaterials for tissue regeneration. *Theranostics*. 2024;14(5):2099–2126. doi:10.7150/thno.93088
36. Ren Y, Nie L, Zhu S, et al. Nanovesicles-mediated drug delivery for oral bioavailability enhancement. *Int J Nanomed*. 2022;17:4861–4877. doi:10.2147/ijn.S382192

37. Castro F, Martins C, Silveira MJ, et al. Advances on erythrocyte-mimicking nanovehicles to overcome barriers in biological microenvironments. *Adv Drug Deliv Rev*. 2021;170:312–339. doi:10.1016/j.addr.2020.09.001
38. Chen C, Wang J, Sun M, et al. Toward the next-generation phyto-nanomedicines: cell-derived nanovesicles (CDNs) for natural product delivery. *Biomed Pharmacother*. 2022;145:112416. doi:10.1016/j.biopha.2021.112416
39. Liu C, Feng Q, Sun J. Lipid nanovesicles by microfluidics: manipulation, synthesis, and drug delivery. *Adv Mater*. 2019;31(45):e1804788. doi:10.1002/adma.201804788
40. Ding Y, Wang L, Li H, et al. Application of lipid nanovesicle drug delivery system in cancer immunotherapy. *J Nanobiotechnology*. 2022;20 (1):214. doi:10.1186/s12951-022-01429-2
41. Yuan X, Li H, Bai H, et al. Synthesis of novel curcumin analogues for inhibition of 11β-hydroxysteroid dehydrogenase type 1 with anti-diabetic properties. *Eur J Med Chem*. 2014;77:223–230. doi:10.1016/j.ejmech.2014.03.012
42. Liu H, Li L, Zhang C, et al. 11β-hydroxysteroid dehydrogenase type 1 inhibitor development by lentiviral screening based on computational modeling. *Pharmacology*. 2018;102(3–4):169–179. doi:10.1159/000491397
43. Duan H, Zhang Q, Liu J, et al. An Integrated Approach Based on Network Pharmacology Combined with Experimental Verification Reveals AMPK/PI3K/Akt signaling is an important way for the anti-type 2 diabetic activity of silkworm excrement. *Diabetes Metab Syndr Obes*. 2021;14:601–616. doi:10.2147/dmso.S291638
44. Bhattacharjee N, Dua TK, Khanra R, et al. Protocatechuic acid, a phenolic from sansevieria roxburghiana leaves, suppresses diabetic cardiomyopathy via stimulating glucose metabolism, ameliorating oxidative stress, and inhibiting inflammation. *Front Pharmacol*. 2017;8:251. doi:10.3389/fphar.2017.00251
45. Hou N, Mai Y, Qiu X, et al. Carvacrol attenuates diabetic cardiomyopathy by modulating the PI3K/AKT/GLUT4 pathway in diabetic mice. *Front Pharmacol*. 2019;10:998. doi:10.3389/fphar.2019.00998
46. Alaaeldin R, Abdel-Rahman IAM, Hassan HA, et al. Carpachromene ameliorates insulin resistance in HepG2 cells via modulating IR/IRS1/PI3k/Akt/GSK3/FoxO1 pathway. *Molecules*. 2021;26(24). doi:10.3390/molecules26247629
47. Hou WL, Yin J, Alimujiang M, et al. Inhibition of mitochondrial complex I improves glucose metabolism independently of AMPK activation. *J Cell Mol Med*. 2018;22(2):1316–1328. doi:10.1111/jcmm.13432
48. Nakae J, Kitamura T, Silver DL, et al. The forkhead transcription factor Foxo1 (Fkhr) confers insulin sensitivity onto glucose-6-phosphatase expression. *J Clin Invest*. 2001;108(9):1359–1367. doi:10.1172/jci12876
49. Sun WX, Lou K, Chen LJ, et al. Lipocalin-2: a role in hepatic gluconeogenesis via AMP-activated protein kinase (AMPK). *J Endocrinol Invest*. 2021;44(8):1753–1765. doi:10.1007/s40618-020-01494-0
50. Farooqui RK, Kaurav M, Kumar M, et al. Permeation enhancer nanovesicles mediated topical delivery of curcumin for the treatment of hyperpigmentation. *J Liposome Res*. 2022;32(4):332–339. doi:10.1080/08982104.2021.2024567
51. Li J, Wu Y, Yuan Q, et al. Gelatin microspheres based on H8-loaded macrophage membrane vesicles to promote wound healing in diabetic mice. *ACS Biomater Sci Eng*. 2024;10(4):2251–2269. doi:10.1021/acsbiomaterials.3c01742